RSC Advances

ROYAL SOCIETY OF CHEMISTRY

www.rsc.org/advances

Synthesis and characterization of ferric tannate as a novel porous adsorptive-catalyst for nitrogen removal from wastewater

Ruina Zhang, Lin Li, Junxin Liu*

Research Center for Eco-Environmental Sciences, Chinese Academy of Sciences, 18 Shuangqing Road, Haidian District, Beijing 100085, China

*To whom correspondence should be addressed. Tel. /Fox: +86 10 62849133. E-mail: jxliu@rcees.ac.cn

Abstract

Ferric tannate has unique adsorption capacities on NH_4^+-N and NO_2^--N simultaneously. So far, no normative method is available for synthesizing ferric tannate. In this work, an optimizing method for synthesizing ferric tannate by using tannic acid and ferric chloride is established under the conditions of room temperature and neutral pH. The optimal molar ratio of tannic acid and ferric chloride were determined to be in the range of 1:20 and 1:25 based on the yield and stability of the ferric tannate composite. Scanning electron microscopy, Brunauer–Emmett–Teller method, X-ray diffraction, and Fourier transform infrared spectrometer were used to characterize the ferric tannate composite. Results showed that the ferric tannate has a rough and porous surface, a large surface area, and an amorphous structure. Experiments of NH_4^+-N and NO_2^--N adsorption reflected that the ferric tannate composite has a unique capacity of adsorption-catalyzed NH_4^+-N and NO_2^--N to N_2. When the mass ratio of NH_4^+-N/ferric tannate and NO_2^--N /ferric tannate were both 200, the removal of NH_4^+-N and NO_2^--N were 98.1% and 96.2%, respectively, after 3.0 hours of reaction. The conversion rate of N_2 increased to 87.1%. Therefore, ferric tannate can be used as a potential material for removing nitrogen from wastewater in the future.

Keywords: Ferric tannate, Synthesis and Characterization, Adsorption performance

Introduction

Nitrogen in wastewater is acknowledged as one of the critical reasons causing severe eutrophication of receiving water bodies. In order to satisfy the strict sewage discharge standards, many technologies for wastewater nitrogen removal have been extensively developed, such as biological nitrogen removal, chemical oxidation, adsorption, and ion exchange. Currently, biological nitrogen removal through combination of aerobic nitrification and anoxic denitrification is widely applied in wastewater treatment plants. However, this approach requires a large amount of oxygen for nitrification, and a sufficient amount of organic substrates to maintain denitrification, which results in high energy consumption.[1] Another biotechnology, anaerobic ammonium oxidation (Anammox), is recognized as a promising alternative for nitrogen removal. In the Anammox process, NO_2^--N is converted to nitrogen gas (N_2) with NH_4^+-N as electron donor; this process consumes less energy and does not require additional carbon substrateas electron donor.[2] However, anammox bacteria exhibits extremely slow growth rate, limiting its widely practical applications.[3, 4]

Chemical approach for nitrogen removal represents a greater reaction rate and higher removal efficiency, but this approach requires additional oxidants or reductants, thereby causing high costs and complicating operational procedures.[5, 6] Adsorption and ion exchange approaches, such as activated carbon and zeolite, can quickly remove NH_4^+-N, NO_2-N, and NO_3-N from wastewater. However, the adsorbent and ion exchange resins must be regenerated after the saturation of adsorbed nitrogen, and the regenerated solution needs further disposal, leading to higher environmental and economical costs.[7-11] Thus, adsorption would be an attractive alternative approach for wastewater nitrogen removal if the adsorbent resin can be regenerated in-situ.

Theoretically, the redox reaction for N_2 production occurs between NH_4^+-N and NO_2-N based on their standard redox potential,[12] but the reaction rate depends on the reaction conditions significantly. Chemical kinetics indicate that the reaction rate can be accelerated through increasing the concentrations of reactants.[13] Adsorption can transform reactants from liquid into solid, causing the reactants to be concentrated on the surface of adsorbents.[14] A very recent patent implied that the presence ferric tannate (a kind of magnetic nanoparticles) is capable of accelerating this reaction at room temperature.[15] Furthermore, a highly cross-linked network of ferric tannate was found to exhibit a rough and porous surface,[16] capable of absorbing both negative and cationic ions due to its ferric ions and negative oxygen ions. In addition, N_2H_4 and NH_2OH are intermediate products in the reaction of NO_2-N and NH_4^+-N,[17-19] while ferric ions can convert N_2H_4 and NH_2OH to N_2.[20-22] Thus, ferric tannate may be used as a novel solution for nitrogen removal. Even though tons of previous studies were illustrated on the development and applications of magnetic nanoparticles in nitrogen removal,[23-25] no literature clearly demonstrated that these magnetic nanoparticles including the ferric tannate, could efficiently eliminate NH_4^+-N and NO_2^--N simultaneously, as well as accelerate the redox reaction between these two substances.

Additionally, no approach has been developed to date for synthesizing the ferric tannate that can be efficiently used in wastewater treatment.

Therefore, this study aims to develop an optimized approach for synthesizing ferric tannate, which can accelerate the reaction between NH_4^+-N and NO_2^--N. Tannic acid and ferric chloride were used as the raw materials to synthesize ferric tannate under the combined condition of room temperature and neutral pH. Moreover, Fourier transform infrared spectrometry (FTIR) and Brunauer–Emmett–Teller (BET) were used to analyze the functional groups and surface morphology of the produced ferric tannate. This study also investigated the potential nitrogen removal performance of ferric tannate in wastewater treatment. The objective of this study is to synthesize a material that can accelerate the reaction between NO_2^--N and NH_4^+-N.

Materials and methods

Materials

Tannic acid and ferric chloride ($FeCl_3$) were used to synthesize ferric tannate. Tannic acid ($C_{76}H_{52}O_{46}$, molar mass: 1701.18 g/mol) was purchased from Sigma-Aldrich Co., USA, with a pure grade of ≥ 99.5%. $FeCl_3$, NH_4Cl, and $NaNO_2$ were purchased from Sinopharm Chemical Reagent Co., China, with a pure grade of ≥ 99%. $NaHCO_3$ was purchased from Tianjin Jinke Fine Chemical Research Institute, China, with a pure grade of ≥ 99.5%. The solutions of tannic acid, $FeCl_3$, and $NaHCO_3$ were prepared with distilled water at concentrations of 0.1, 1, and 0.65 mol/L, respectively.

Synthesis of ferric tannate

Tannic acid is an abundant polyphenolic compound. Its orthophenolic hydroxyl structure can cause complexation reactions with ferrous and ferric ions, which form a hybrid with metal-organic framework. The chemical structures of tannic acid and ferric tannate are shown in Fig.1.[26, 27] In view of the complexity of the chemical structure of tannic acid, six molar ratios of tannic acid and $FeCl_3$ (1:10, 1:15, 1:20, 1:25, 1:30, 1:40) were chosen to investigate the influence of varying proportions on ferric tannate yield. The synthesis of ferric tannate was performed in a conical flask with a volume of 150 mL. An amount of 10 mL of 0.1 mol/L tannic acid solutions was mixed with various volumes of 1 mol/L $FeCl_3$ solution. The pH of the mixture was adjusted to 7 by using 0.65 mol/L $NaHCO_3$ solution. The reaction products were separated via sedimentation, and the resultant precipitation was washed with deionized water for four times, centrifuged (3000 rpm, 2 min), and dried in a freezer dryer at −50 °C.

Characterization of ferric tannate

The ferric tannate yield (y_e) was calculated by the following equation (eq. 1):

$$y_e = \frac{m_{ft}}{(m_t + m_{fe})} \times 100\% \quad (1)$$

where m_{ft} is the weight of the ferric tannate (mg); m_t and m_{fe} are the weights of tannic acid and ferric chloride (mg), respectively.

To determine the stability of ferric tannate yield, 0.2 g ferric tannate composition,

which was prepared with different ratios as mentioned earlier, was placed into six shake flasks. Then, each shake flask was charged with 200 mL of deionized water. After 1 h of continuous stirring, the mixture in each shake flask was filtered through a 0.45 μm pore size filter. The filtrate was measured with a UV-vis spectrophotometer (UV-1700, Hitachi Co., Japan) in 200 nm to 500 nm wavelength.

Field emission scanning electron microscopy (FE-SEM), which was coupled with an energy dispersive X-ray spectroscopy (EDS) detector (SU-8020, Hitachi Co., Japan), was employed to observe the surface physical morphology and major elements of ferric tannate.

An automatic micropore and mesopore analyzer (ASAP 2020 HD88, USA) was operated to analyze the specific surface area and pore size distribution of ferric tannate. Moreover, the specific surface area and pore size distribution of the ferric tannate were determined with N_2 adsorption isotherm at 77 K by using Micromeritics ASAP 2010 accelerated surface area analyzer and BET method.[28]

Fourier transform infrared spectrometer (FTIR, Tensor 27, Germany) was applied to measure the functional group of tannin acid and ferric tannate with potassium bromide pellet method in the range of 400 cm^{-1} to 4000 cm^{-1} region.[29]

X-ray diffraction (XRD; X'Pert PRO MPD, PA Nalytical, Holland) was used to analyze the purity and crystallinity of ferric tannate, ferric chloride, and tannic acid with Cu-Kα radiation (λ=0.015418 nm) in the 2θ range of 10° to 80°. The XRD data were collected in a scan mode with a step length of 0.5 with a scanning rate of 6 °/min. The accelerating voltage and the applied current were 45 kV and 45 mA, respectively.

Determination of the nitrogen removal performance

Several batch tests were conducted in stoppered conical flasks to estimate the nitrogen removal performance of the synthesized ferric tannate. Stock solutions were prepared by dissolving NH_4Cl or/and $NaNO_2$ in deionized water. For each time, 0.1 g ferric tannate and 50 mL stock solutions were mixed in a flask, which was then shaken with a shaker at 200 rpm at room temperature. In the procedure of the nitrogen removal by using ferric tannate, the pH was 7, which was adjusted with HCl or $NaHCO_3$.[30]

In adsorption isotherm studies, the stock solutions with different initial concentrations of NH_4^+-N or NO_2^--N were added into 100 mL conical flasks, and the equilibrium time was set to 2 h. The samples were separated via filtration.

In the experiments, both concentrations of NH_4^+-N and NO_2^--N in the reaction solution were 50 mg/L. The amounts of 100 mL stock solution and 1.0 g ferric tannate were added into a 150 mL stoppered conical flask. Then, the flask was shaken at 200 rpm for 3.0 h at room temperature, and the 500 μL water samples and 50 μL gas samples were collected every 20 min. In the study, the data of NH_4^+ and NO_2^- adsorption on the ferric tannate at room temperature were achieved through three groups of parallel tests.

The concentrations of NH_4^+-N and NO_2^--N were measured according to standard methods.[31] The Agilent 6890N Gas Chromatograph equipped with TCD detector was used to analyses the content of N_2.

The adsorption amount of NH_4^+-N or NO_2^--N on the ferric tannate at equilibrium, q_e (mg-N/g), was calculated with the following equation (eq. 2 and eq. 3):

$$q_e = \frac{(C_i - C_e)V}{m} \quad (2)$$

$$\text{Removal} = \frac{(C_i - C_e)}{C_i} \times 100\% \quad (3)$$

Where q_e is the equilibrium amount of adsorption on the adsorbent surface (mg/g), C_i and C_e are the initial and equilibrium concentrations of NH_4^+-N or NO_2^--N (mg-N/L) in the solution, respectively. V is the volume of the solution (L), and m is the weight of the ferric tannate (g).

The Langmuir adsorption equation and the Freundlich adsorption equation can be linearised according to the equation. [32]

Due to the inherent bias resulting from linearisation of the isotherm model, the error analysis was employed as a criterion for the fitting quality. This statistical analysis is based on the sum of the squares of the differences between the experimental and the Langmuir model and Freundlich model calculated data. The error was calculated as the following equation (eq. 4 and eq. 5):

$$\text{Relative error} = \frac{\sum_{i=1}^{n}\left|\frac{q_i - q_{sim}}{q_i}\right|}{n} \times 100\% \quad (4)$$

$$\text{Standard deviation} = \sqrt{\frac{1}{n}\sum_{i=1}^{n}\left(\left|\frac{q_i - q_{sim}}{qi}\right| - \frac{1}{n}\sum_{i=1}^{n}\left|\frac{q_i - q_{sim}}{q_i}\right|\right)^2} \quad (5)$$

where q_i the equilibrium capacity of the adsorbent obtainedfrom experiment (mg/g), q_{sim} was the simulated adsorption capacities which calculated with Langmuir equation and Freundlich equation (mg/g).

A low value of the relative error or standard deviation indicates that experimental data fit better to the value from the model. In order to confirm the best-fit isotherms and kinetic models for the adsorption system, there is a need to analyse the data set using the Nash-Sutcliffe efficiency (NSE).[33, 34] As a dimensionless goodness-of-fit indicator, the values of NSE could be widely used and potentially reliable statistic for assessing the goodness of fit of isothermal adsorption models. NSE = 1 indicated a perfect fit, $0.75 \leqslant \text{NSE} \leqslant 0.9$ suggested a good fit, $0.65 \leqslant \text{NSE} \leqslant 0.749$ suggested a acceptable fit. NSE is calculated as follows (eq. 6):

$$\text{NSE} = 1 - \frac{\sum_{i=1}^{n}(q_i - q_{sim})^2}{\sum_{i=1}^{n}(q_i - \bar{q})^2} \quad (6)$$

Where q_i is the equilibrium capacity of the adsorbent obtained from experiment (mg/g), q_{sim} is the simulated adsorption capacities (mg/g), $\bar{q}$ was the average adsorption capacities (mg/g).

Synthesis of ferric tannate

As expected, the reaction of tannic acid with $FeCl_3$ resulted in the formation of an abundant precipitate ferric tannate. Table 1 presents a summary of the results of the ferric tannate yield in the six proportions of tannic acid and $FeCl_3$, which showed an obvious response between the ratio of tannic acid and $FeCl_3$ and ferric tannate yield.

Increasing the proportions of tannic acid and $FeCl_3$ from 1:10 to 1:30 resulted in the gradual increase of ferric tannate yields. The highest yield, 82.6%, appeared in the case of 1:30. Moreover, ferric tannate yields are nearly equal in the cases of 1:20, 1:25, and 1:40.

The stability of the ferric tannate composition in liquid will be highly important to apply nitrogen removal from wastewater. Therefore, the dissolution of the ferric tannate compositions in water was determined. The UV-visible adsorbance spectra of the soak water of the ferric tannate composition are shown in Fig.2. The results showed that nothing could be dissolved in the cases of 1:15, 1:20, and 1:25, but the adsorption peak appeared at 302 nm in the case of 1:10 and at 303 nm in the cases of 1:30 and 1:40, which indicated that some substrates were dissolved into the water.

The preceding results indicated that the molar ratio of tannic acid to ferric ion was responsible for the formation of the ferric tannate complex. With strong reducibility, the phenolic hydroxyl in tannic acid can reduce Fe^{3+} to Fe^{2+}.[35-37] In the case of 1:10, the excess tannic acid can produce a dissolved ferrous tannate, whose adsorption peak appeared at 302 nm.[38] In the cases of 1:30 and 1:40, the ferric ion was in excess, which could lead to the formation of $Fe(OH)_3$. Therefore, the adsorption peak at 303 nm is probably the ferric ion dissolution.[39] Therefore, based on the yield and stability of the ferric tannate composition, the optimal molar ratios of tannic acid and $FeCl_3$ to synthesize ferric tannate are between 1:20 and 1:25.

Characterization of ferric tannate

According to the results of the preceding experiment, the synthesizing sample in the case of 1:20 was selected to characterize ferric tannate composite. FE-SEM images of the ferric tannate composite are illustrated in Fig.3. The ferric tannate composite had a rough and porous surface structure. The adsorption isotherms of N_2 on the ferric tannate composite were used to deduce the surface characteristics. The results showed that the BET surface area, pore volume, and average pore diameter were 97 m^2/g, 0.073 cm^3/g, and 66.58 nm, respectively. In general, a large surface area and pore diameter can increase the adsorption capacity of the material.[40, 41]

The SEM-EDS spectrum of the ferric tannate composite is shown in Fig.4. The composite mainly consists of C, O, and Fe elements, and the percentage contents of C, O, and Fe in the ferric tannate composite are 23.06%, 46.83%, and 29.91%, respectively. However, the ratio of C and O from the SEM-EDS spectrum is anomalous compared with the chemical formula of tannic acid ($C_{76}H_{52}O_{46}$). A possible explanation is that ferric ion occurs partially hydrolysis reaction at neutral pH condition, which leads to an increase of O in the ferric tannate composite.[35, 42, 43] However, this finding should be verified at further research.

The XRD patterns of the tannic acid, $FeCl_3$, and ferric tannate composite was shown inFig.5. XRD data indicate that $FeCl_3$ has many diffraction peaks because of its crystalline structure.[44] The diffraction peaks of the tannic acid and ferric tannate composite appear in $2\theta=20°$ to 30° range, which demonstrate that they have amorphous structure.

The FTIR spectra of the tannic acid and ferric tannate composite are illustrated in Fig.6. Two broad adsorption bands in the 3600 cm^{-1} to 3100 cm^{-1} range that indicated the presence of phenolic hydroxyl group were observed, and the band at 1320 cm^{-1} exhibits a characteristic of the bending vibrations of O-C in phenolic hydroxyl group. The sharp band at 1400 cm^{-1} in the spectra of the ferric tannate composite is very pronounced, which ascribed to C=O of benzoic acid vibration adsorption peaks. This phenomenon can be explained by the chelation and redox reaction of Fe^{3+} with phenolic hydroxyl, which results in a coexistence of Fe^{3+} and Fe^{2+} in ferric tannate.[27, 35] The interaction between Fe^{3+} and the phenolic hydroxyl group has effect on the O-C bond stretch vibration, in which the band shifted from 1320 cm^{-1} in the spectra of the tannic acid to 1338 cm^{-1} to 1375 cm^{-1} in the spectra of the ferric tannate composite.[45-47] During the combination process of Fe^{3+} with the phenolic hydroxyl group, oxygen anion was formed.

Valuation of the nitrogen removal performance of ferric tannate composite

Some batch tests adsorbing NH_4^+-N and NO_2^--N were conducted separately to estimate the nitrogen removal performance of the synthesized ferric tannate. The data of NH_4^+-N and NO_2^--N adsorption on the ferric tannate composites, only NH_4^+-N or NO_2^--N in the solution, were shown in Fig.7. Langmuir and Freundlich models were usually used to describe the equilibrium isotherm data. The results from linear of these isotherms of NH_4^+-N and NO_2^--N on the ferric tannate composites were listed in Table 2. Compared with the correlation coefficient value of the linear plot of the Freundlich isotherm, that of Langmuir model was in better agreement with observed data (R^2=0.990 for NH_4^+-N adsorption and R^2=0.957 for NO_2^--N adsorption). The maximum adsorption capacities of NH_4^+-N and NO_2^--N calculated from the Langmuir equations were 13.6 mg/g and 10.2 mg/g at room temperature, respectively. The results indicated that the adsorption capacity of ferric tannate toward NH_4^+-N was better than that toward NO_2^--N.

In the study, the values of NSE (Table 3) indicated that the Langmuir models of NH_4^+-N and NO_2^--N being considered very good ($0.9 \leqslant NSE \leqslant 1$). The Freundlich models of NH_4^+-N and NO_2^--N being considered good ($0.8 \leqslant NSE \leqslant 0.9$) and very good ($0.9 \leqslant NSE \leqslant 1$), respectively.

Adsorption performances of ferric tannate toward NH_4^+-N and NO_2^--N were different and varied significantly with time. Fig.8 showed the adsorptive behaviors for NH_4^+-N or/and NO_2^--N of ferric tannate. The concentration of NH_4^+-N and NO_2^--N decreased with time, while the production of N_2 increased at the same time (Fig.8). When the mass ratio of NH_4^+-N/ferric tannate and NO_2^--N /ferric tannate were both 200, the removal of NH_4^+-N and NO_2^--N were 98.1% and 96.2%, respectively, after 3.0 hours of reaction. The conversion rate of N_2 increased to 87.1%. Results showed that after the addition of ferric tannate, the removal of NH_4^+-N and NO_2^--N increased obviously with N_2 production increased simultaneously, which indicated that ferric tannate would be benefit for the reaction between NH_4^+-N and NO_2^--N, and lead to more N_2 generation. These results indicated that the ferric tannate had a unique

capacity to absorb anions and cations simultaneously, and an adsorption-catalyzed reaction occurred on the ferric tannate with the adsorption of NH_4^+-N and NO_2^--N. The adsorption-catalyzed reaction between NH_4^+-N and NO_2^--N could refresh the adsorption site of ferric tannate, and the continuous adsorption of NH_4^+-N and NO_2^--N on ferric tannate could be promoted. Thus, the removal amount of NH_4^+-N and NO_2^--N was enhanced. Therefore, the ferric tannate may be used as a promising material to remove nitrogen from wastewater in the future.

In the practical use, the dosage of ferric tannate will be adjusted with the concentrations of NH_4^+-N and NO_2^--N in the wastewater, for the purpose of more NH_4^+-N and NO_2^--N converted to N_2.

Conclusions

A novel method to synthesize porous ferric tannate composites was demonstrated by using tannic acid and ferric chloride under the conditions of room temperature and neutral pH. According to the yield and stability of the ferric tannate composite, the optimal molar ratio of tannic acid and $FeCl_3$ is between 1:20 and 1:25. Combined with the characterization of SEM and BET, the characteristics of porous surface and large surface area of the ferric tannate composite were confirmed. XRD analysis confirmed that the ferric tannate composite has amorphous structure. The adsorption test results indicated that the adsorption of NH_4^+-N and NO_2^--N on the ferric tannate composite agrees well with that obtained Langmuir model. Moreover, the maximum adsorption capacity of NH_4^+-N and NO_2^--N calculated from the Langmuir equations were 13.6 mg/g and 10.2 mg/g at room temperature, respectively. Furthermore, ferric tannate has a unique capacity to absorb NH_4^+-N and NO_2^--N simultaneously. In addition, an adsorption-catalyzed reaction can occur on the ferric tannate with the adsorption of NH_4^+-N and NO_2^--N, which enhances the removal of NH_4^+-N and NO_2^--N. When the mass ratio of NH_4^+-N/ferric tannate and NO_2^--N /ferric tannate were both 200, the removal of NH_4^+-N and NO_2^--N were 98.1% and 96.2%, respectively, after 3.0 hours of reaction. The conversion rate of N_2 increased to 87.1%. Therefore, ferric tannate may be used as a promising material to remove nitrogen from wastewater in the future.

Acknowledgments

This study was financially supported by the National Science Foundation of China (Nos. 51138009 and 51208459).

References

1 A. Dey, *Environmental Engineering Science*, 2010, 27, 757-765.

2 B. Kartal, J. G. Kuenen and M. C. M. van Loosdrecht, *Science*, 2010, 328, 702-703.

3 M. Strous, J. J. Heijnen, J. G. Kuenen and M. S. M. Jetten, *Applied Microbiology and Biotechnology*, 1998, 50, 589-596.

4 K. Isaka, Y. Date, T. Sumino, S. Yoshie and S. Tsuneda, *Applied Microbiology and Biotechnology*, 2006, 70, 47-52.

5 I. Ihara, K. Umetsu, K. Kanamura and T. Watanabe, *Bioresource Technology*, 2006, 97, 1360-1364.

6 Y. H. Liou, S. L. Lo, C. J. Lin, W. H. Kuan and S. C. Weng, *Journal of Hazardous Materials*, 2005, 127, 102-110.

7 G. D. Ji, Y. Zhou and J. J. Tong, *Environmental Engineering Science*, 2010, 27, 871-878.

8 P. A. Terry, *Environmental Engineering Science*, 2009, 26, 691-696.

9 S. Annouar, M. Mountadar, A. Soufiane, A. Elmidaoui and M. A. M. Sahli, *Desalination*, 2004, 165, 437-437.

10 S. Leakovic, I. Mijatovic, S. Cerjan-Stefanovic and E. Hodzic, *Water Research*, 2000, 34, 185-190.

11 H. Zheng, L. Han, H. Ma, Y. Zheng, H. Zhang, D. Liu and S. Liang, *Journal of Hazardous Materials*, 2008, 158, 577-584.

12 J. C. Fanning, *Coordination Chemistry Reviews*, 2000, 199, 159-179.

13 S. J. Klippenstein, V. S. Pande and D. G. Truhlar, *Journal of the American Chemical Society*, 2014, 136, 528-546.

14 X. F. Wu, Y. L. Hu, F. Zhao, Z. Z. Huang and D. Lei, *Journal of Environmental Sciences-China*, 2006, 18, 1167-1175.

15 Y. Yuasa, Jpn Kakai JP 197 196[87 197196] 31 Aug 1987.

16 H. Wilson, C. Carr and M. Hacke, *Chemistry Central Journal*, 2012, 6.

17 D. A. Nguyen, M. A. Iwaniw and H. S. Fogler, *Chemical Engineering Science*, 2003, 58, 4351-4362.

18 W. R. L. van der Star, M. J. van de Graaf, B. Kartal, C. Picioreanu, M. S. M. Jetten and M. C. M. van Loosdrecht, *Applied and Environmental Microbiology*, 2008, 74, 4417-4426.

19 B. Kartal, W. J. Maalcke, N. M. de Almeida, I. Cirpus, J. Gloerich, W. Geerts, H. J. M. O. den Camp, H. R. Harhangi, E. M. Janssen-Megens, K. J. Francoijs, H. G. Stunnenberg, J. T. Keltjens, M. S. M. Jetten and M. Strous, *Nature*, 2011, 479, 127-U159.

20 J. Mondal, K. T. Nguyen, A. Jana, K. Kurniawan, P. Borah, Y. L. Zhao and A. Bhaumik, *Chemical Communications*, 2014, 50, 12095-12097.

21 Z. M. Peng, M. Z. Wu, Y. Xiong, J. Wang and Q. W. Chen, *Chemistry Letters*, 2005, 34, 636-637.

22 Y. P. He, Q. L. Sheng, B. Liu and J. B. Zheng, *Electrochimica Acta*, 2012, 66,

82-87.
23 Y. Liu, J. Zhou, J. Gong, W. P. Wu, N. Bao, Z. Q. Pan and H. Y. Gu, *Electrochimica Acta*, 2013, 111, 876-887.
24 O. Gutfleisch, M. A. Willard, E. Bruck, C. H. Chen, S. G. Sankar and J. P. Liu, *Advanced Materials*, 2011, 23, 821-842.
25 S. Rakshit, C. J. Matocha and G. R. Haszler, *Journal of Environmental Quality*, 2005, 34, 1286-1292.
26 A. T. Iffat, Z. T. Maqsood and N. Fatima, *Journal of the Chemical Society of Pakistan*, 2005, 27, 174-177.
27 T. K. Ross and R. A. Francis, *Corrosion Science*, 1978, 18, 351-361.
28 Q. L. Hongsen Zhang, Jun Wang, Jingyuan Liu, *RSC Advances*, 2015, 5, 8.
29 F. Elkabbany, Y. Badr and M. Tosson, *Physica Status Solidi a-Applied Research*, 1981, 63, 699-704.
30 A. Ritter and A. Peppas, Journal of Controlled Release, 1987, 37-42.
31 M. H. Mccrady, *American Journal of Public Health and the Nations Health*, 1966, 56, 684-&.
32 V. Vimonses, S. M. Lei, B. Jin, C. W. K. Chowd and C. Saint, *Chemical Engineering Journal*, 2009, 148, 354-364.
33 A. Ritter and R. Munoz-Carpena, *Journal of Hydrology*, 2013, 480, 33-45.
34 L. Wu, R. Munoz-Carpena, B. Gao, W. Yang and Y. A. Pachepsky, *Environmental Science & Technology*, 2014, 48, 3883-3890.
35 J. A. Jaen, J. De Obaldia and M. V. Rodriguez, *Hyperfine Interactions*, 2011, 202, 25-38.
36 R. Y. Liu and A. W. Xu, *Rsc Advances*, 2014, 4, 40390-40395.
37 G. K. B. Lopes, H. M. Schulman and M. Hermes-Lima, *Biochimica Et Biophysica Acta-General Subjects*, 1999, 1472, 142-152.
38 A. H. Basaran and O. H. Tuovinen, *Applied Microbiology and Biotechnology*, 1986, 24, 338-341.
39 X. M. Li, T. T. Shen, D. B. Wang, X. Yue, X. Liu, Q. Yang, J. B. Cao, W. Zheng and G. M. Zeng, *Journal of Environmental Sciences-China*, 2012, 24, 269-275.
40 C. L. Mangun, M. A. Daley, R. D. Braatz and J. Economy, *Carbon*, 1998, 36, 123-129.
41 L. B. Kong, H. Li, J. Zhang, Y. C. Luo and L. Kang, *Applied Surface Science*, 2010, 256, 6688-6693.
42 J. A. Jaen and C. Navarro, *Hyperfine Interactions*, 2009, 192, 61-67.
43 R. S. Peres, E. Cassel, C. A. Ferreira and D. S. Azambuja, *Industrial & Engineering Chemistry Research*, 2014, 53, 2706-2712.
44 Y. Zhang, Z. X. Zhang, T. B. Li, X. G. Liu and B. S. Xu, *Spectrochimica Acta Part a-Molecular and Biomolecular Spectroscopy*, 2008, 70, 1060-1064.
45 E. G. ı. d. S. n. J.A. Ja´en , C. Hern´andez *Hyperfine Interactions*, 1999, 122, 8.
46 A. T. Iffat, Z. T. Maqsood, K. Ali and S. Nisar, *Journal of the Chemical Society of Pakistan*, 2004, 26, 151-156.

47 J. Iglesias, E. G. De Saldana and J. A. Jaen, *Hyperfine Interactions*, 2001, 134, 109-114.
48 R. G. Andrade, J. S. Ginani, G. K. B. Lopes, F. Dutra, A. Alonso and M. Hermes-Lima, *Biochimie*, 2006, 88, 1287-1296.

Figure captions

Fig.1 Schematic diagram of chemical structures of (a) tannic acid and (b) ferric tannate.

Fig.2 UV-visible absorbance spectra of the soak water of the ferric tannate composite.

Fig.3 SEM of for 1:20 tannic acid/$FeCl_3$ (a) ferric tannate composition and (b) its microstructure.

Fig.4 SEM-EDS spectrum of the ferric tannate composite (1:20 tannic acid/$FeCl_3$).

Fig.5 XRD spectra of the tannic acid, $FeCl_3$ and ferric tannate composite (1:20 tannic acid/$FeCl_3$).

Fig.6 FTIR spectra of tannin and ferric tannate (1:20 tannic acid/$FeCl_3$).

Fig.7 Adsorption isotherm of NH_4^+-N and NO_2^--N on ferric tannate.

Fig.8 The removal of NH_4^+-N and NO_2^--N and the conversion rate of N_2 with the addition of ferric tannate.

Table 1 Yield of ferric tannate at different ratio of tannic acid and $FeCl_3$.

Ratio(Tannic acid/$FeCl_3$)	1:10	1:15	1:20	1:25	1:30	1:40
Yield (%)	71.3	75.4	78.4	79.2	82.6	78.4

Table 2 Langmuir and Freundlich isotherm parameters for NH_4^+-N and NO_2^--N adsorption by ferric tannate.

	Langmuirparameters			Freundich parameters		
	K_L(L/mg)	q_m(mg/g)	R^2	K_F [(mg/g)/(mg/L)^n]	n	R^2
NH_4^+-N	0.079	13.9	0.990	7.06	0.109	0.860
NO_2^--N	0.009	10.2	0.957	2.84	4.53	0.952

Table 3 The data of error estimation and NSE

	Error estimation (%)				NSE			
	Langmuir		Freundlich		Langmuir		Freundlich	
	NH_4^+	NO_2^-	NH_4^+	NO_2^-	NH_4^+	NO_2^-	NH_4^+	NO_2^-
Test1	1.51±1.24	1.46±1.44	3.50±2.28	2.94±2.07	0.972	0.994	0.854	0.992
Test2	1.58±0.901	1.67±1.19	3.51±2.32	2.74±2.29	0.976	0.996	0.849	0.991
Test3	1.89±1.19	2.42±1.44	3.85±2.63	1.60±1.43	0.965	0.994	0.824	0.997

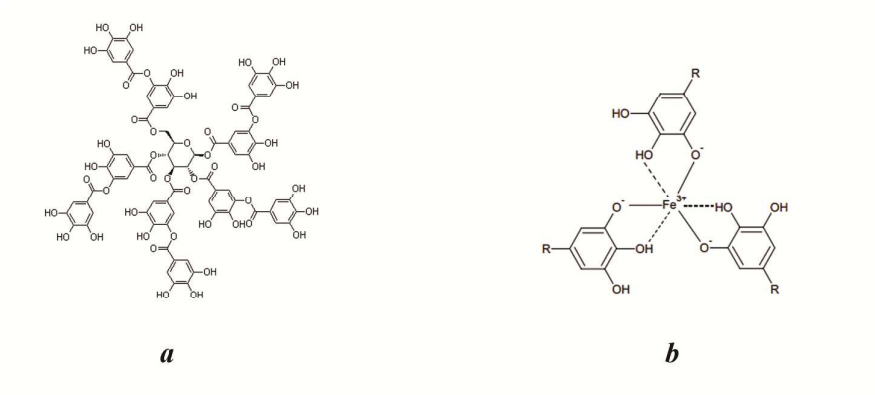

Fig.1 Schematic diagram of chemical structures of (a)tannic acid and (b) ferric tannate

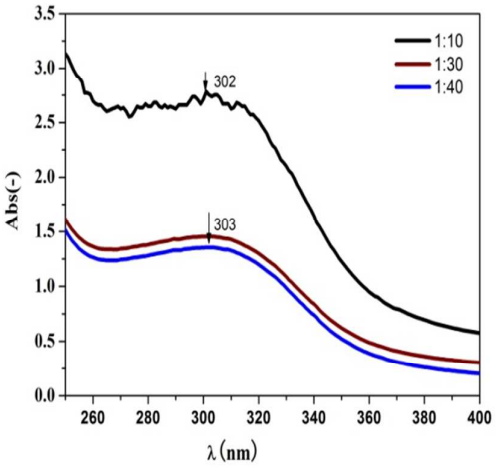

Fig. 2 UV-visible adsorbance spectra of the soak water of the ferric tannate composite.

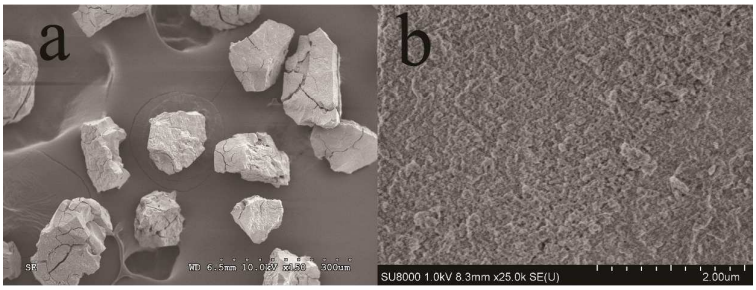

Fig. 3 SEM of for 1:20 tannic acid/$FeCl_3$(a)ferric tannate composition and (b)its

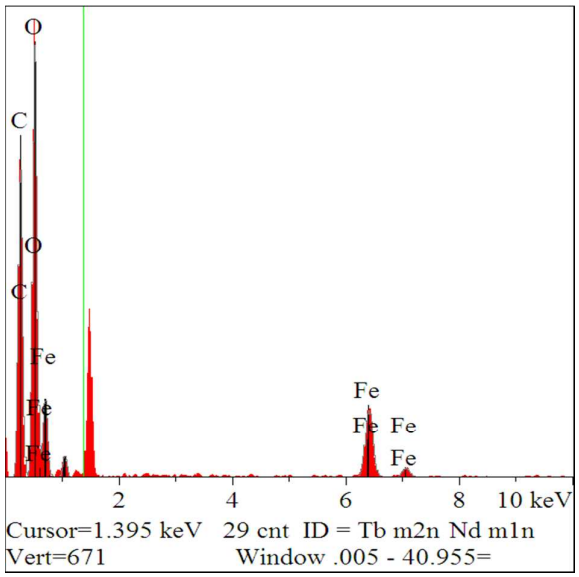

Fig.4 SEM-EDS spectrum of the ferric tannate composite (1:20 tannic acid/$FeCl_3$)

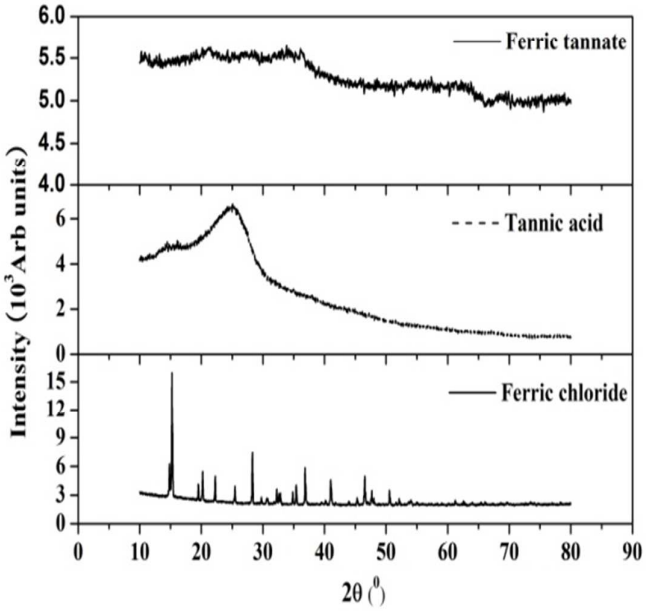

Fig. 5 XRD spectra ofthe tannic acid, $FeCl_3$ and ferric tannate composite (1:20 tannic acid/$FeCl_3$).

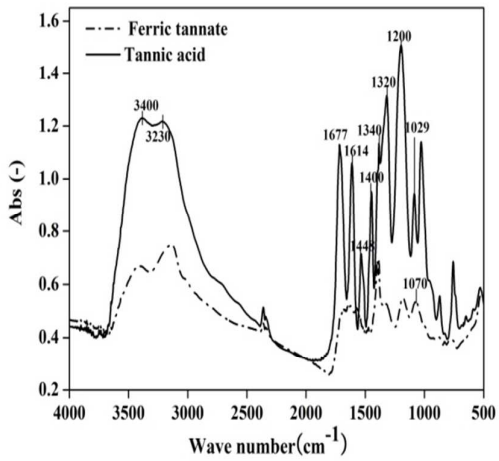

Fig.6 FTIR spectra of tannin and ferric tannate (1:20 tannic acid/$FeCl_3$)

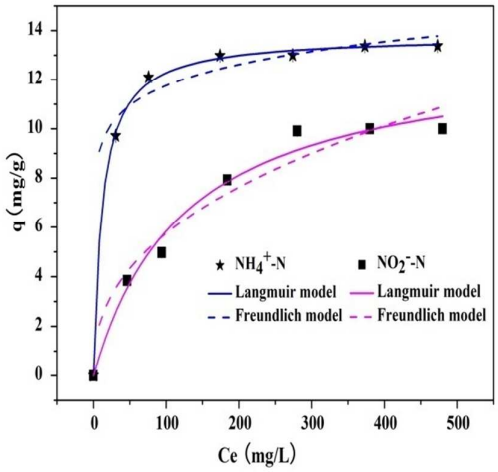

Fig.7 Adsorption isotherm of NH_4^+-N and NO_2^--N onferric tannate

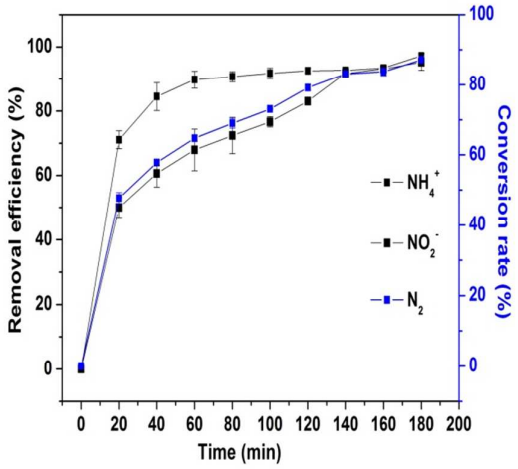

Fig.8 The removal of NH_4^+-N and NO_2^--N and the conversion rate of N_2 with the addition of ferric tannate